Geometry of the Retinal Nerve Fibers From Emmetropia Through to High Myopia at Both the Temporal Raphe and Optic Nerve

Phillip Bedggood,[1] Soumya Mukherjee,[1] Bao N. Nguyen,[1] Andrew Turpin,[2] and Allison M. McKendrick[1]

[1]Department of Optometry and Vision Sciences, The University of Melbourne, Parkville, Victoria, Australia
[2]School of Computing and Information Systems, The University of Melbourne, Parkville, Victoria, Australia

Correspondence: Phillip Bedggood, c/o Department of Optometry and Vision Sciences, The University of Melbourne, Melbourne 3010 Australia;
pabedg@unimelb.edu.au.

Submitted: May 16, 2019
Accepted: October 7, 2019

Citation: Bedggood P, Mukherjee S, Nguyen BN, Turpin A, McKendrick AM. Geometry of the retinal nerve fibers from emmetropia through to high myopia at both the temporal raphe and optic nerve. *Invest Ophthalmol Vis Sci*. 2019;60:4896–4903. https://doi.org/10.1167/iovs.19-27539

Purpose. The geometry of retinal nerve fibers may be altered with myopia, a known risk factor for glaucoma. Recent developments in high resolution imaging have enabled direct visualization of nerve fiber bundles at the temporal raphe with clinical hardware, providing evidence that this area is sensitive to glaucomatous damage. Here, we test the hypothesis that nerve fiber geometry is altered by myopia, both at the temporal raphe and surrounding the optic nerve head.

Methods. Seventy-eight healthy individuals participated, with refractive errors distributed between emmetropia and high myopia (+0 to −13 DS). Custom high-density OCT scans were used to visualize RFNL bundle trajectory at the temporal raphe. A standard clinical OCT protocol was used to assess papillary minimum rim width (MRW) and peripapillary retinal nerve fiber layer (RNFL) thickness.

Results. Measures of raphe shape—including position, orientation, and width—did not depend significantly on axial length. In 7.5% of subjects, the raphe was rotated sufficiently that inversion of structure-function mapping to visual field space is predicted in the nasal step region. Low concordance to ISNT and related rules was observed in myopia (e.g., for RNFL, 8% of high axial myopes compared with 67% of emmetropes). Greater robustness to refractive error was observed for the IT rule.

Conclusions. High density OCT scans enabled visualization of marked interindividual variation in temporal raphe geometry; however, these variations were not well predicted by degree of myopia as represented by axial length. That said, degree of myopia was associated with abnormal thickness profiles for the papillary and peripapillary nerve fiber layer.

Keywords: temporal raphe, ISNT rule, myopia, glaucoma

For reasons that are poorly understood, myopia increases the risk of developing glaucoma.[1] It is possible that progressive axial elongation of the eye exerts biomechanical stress on the axons of retinal ganglion cells, resulting in thinning of the peripapillary nerve fiber layer (RNFL) or deviations to the trajectory of nerve fiber bundles. These factors could in turn indicate susceptibility to other glaucomatous stressors. Regardless of any role played by biomechanical stress, myopic eyes differ in shape from nonmyopic eyes, which can potentially change the interpretation of clinical tests in the context of glaucoma management; therefore, it is important to understand precisely how retinal tissue changes shape with myopia. These considerations are expanded upon below.

Characteristic loss of RNFL thickness is a hallmark of glaucomatous damage,[2] and is widely relied upon in clinical assessment.[3,4] In the absence of longitudinal data for a given patient, comparisons are made to the expected normal pattern of RNFL thickness. The ISNT rule specifies that thickness should be greatest inferiorly, then superiorly, nasally, and temporally. This rule is often violated in the healthy eye for both neuroretinal rim and peripapillary RNFL measures; however, variations such as IST and IS are obeyed in a majority of patients.[5] In myopia, concordance with the ISNT rule may be even less prevalent, with a recent study reporting concordance of only 12% with the ISNT rule for RNFL thickness.[6] This agrees with other studies that have shown changes in the position of peak thickness of the peripapillary RNFL in myopia.[7,8]

In addition to overt changes in RNFL thickness, biomechanical forces during axial elongation could lead to deviation of the trajectory of retinal nerve fibers. Axons of each retinal ganglion cell trace out either a superior or inferior course as they travel to the optic disc. In the temporal retina, the axis of symmetry between superior and inferior bundles is known as the "nerve fiber raphe."[9] Recent developments allow direct visualization of the temporal raphe,[10,11] including widely available clinical instrumentation such as spectral domain optical coherence tomography (OCT),[12] with imaging settings used routinely in the clinic.[13] In some individuals, there is significant departure from an assumed horizontal raphe.[10–12,14] Clinically, the raphe position is relevant to the combined assessment of functional (e.g., visual field) and structural (e.g., OCT) data.[15–17] Small deviations in the axis of symmetry can cause a point in visual space previously thought to map to one hemisphere of the optic disc, to, in fact, "flip"

to the opposite side.[18] Hence, the anatomy of the temporal raphe may be relevant to improving the assessment of glaucoma.[11,13,14,18–22] Furthermore, the low density of RNFL bundles in this area may enable direct visualization of changes to bundle density. Glaucomatous deficits occur characteristically in this region, which corresponds to the nasal step of the visual field.[23] The orientation of the raphe may also be relevant for the assessment of other neuroretinopathy; for example, a localized vascular infarct may appear to cross the midline and so appear to have a different or nonlocalized cause.

Previous studies using higher resolution imaging of the raphe have included few participants (e.g., $N = 15$ to 25)[12,22,24] or have not employed a range of refractive errors,[21] thereby making it unclear whether axial elongation of the eye is an important determinant of the geometry of retinal nerve fiber bundles at the raphe. However, there is good reason to investigate this issue, given differences in fiber distribution at the disc as previously noted in myopia.[7,8] Interindividual variation in the temporal raphe could not only include differences in orientation[14,24] but also in displacement of the raphe from the fovea-horizontal axis (which we term "displacement") or in increased width of the apparent fiber-free zone between hemifields (the raphe "gap").[10,11]

Here we used a custom high-density OCT scanning protocol to visualize the temporal raphe in healthy eyes that have varying degrees of myopia in addition to using standard clinical scans to measure peripapillary RNFL and papillary minimum rim width (MRW). We tested the general hypothesis that the degree of myopia, as represented by axial length, influences the normal geometry of the retinal nerve fibers. The specific hypotheses tested were:

1. Myopia alters the normal trajectory of retinal nerve fiber bundles temporal to the macula.
2. Myopia alters the normal thickness pattern of the retinal nerve fiber layer nearby and surrounding the optic disc.

Materials and Methods

Seventy-eight healthy participants were recruited, based on detection of a significant correlation between our outcome measures and degree of myopia corresponding to $R^2 > 0.1$, with probability for Type I error < 0.05 and probability for Type II error < 0.20.

All subjects were provided written informed consent. All procedures complied with the tenets of the Declaration of Helsinki and were approved by the Human Research Ethics Committee of the University of Melbourne.

Mean subject age was 25 years (range, 18–35) and spherical equivalent (SE) ranged from 0D to −13D (minimum 10 subjects per 1D range of refraction between 0D to −5D; 27 subjects in the range −3 to −6D; 17 subjects beyond −6D). Axial length and vitreous chamber depth (VCD) were measured by A-scan ultrasonography (AL-100 biometer; Tomey GmbH, Nürnberg, Germany).

In addition to statistical analysis of the influence of axial length as a continuous variable, described below, we also performed analysis for 2 "extreme" groups in our data:

1. "Emmetropes" who did not exceed a refractive error criterion[25] of –0.75 DS in both primary meridia ($n = 12$; axial length = 22.9 ± 1.0 mm).
2. "High axial myopes" who had spherical equivalent ≤–6.00 D and axial length ≥26.0 mm ($n = 12$; axial length = 27.2 ± 0.8 mm).[26]

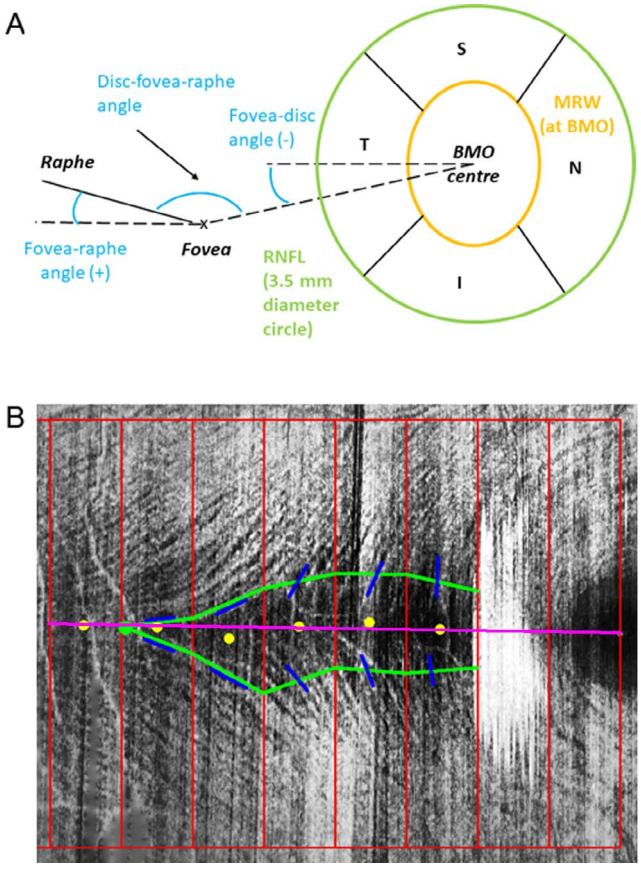

Figure 1. Key anatomical definitions used. (**A**) The sign convention adopted for specifying the relative geometry of the fovea, disc, and temporal raphe (*blue*), and the measurement zones for minimum rim width (*orange*), and retinal nerve fiber layer thickness (*green*). (**B**) The assessment of raphe shape according to a straight line approximation (*magenta*), local displacement from the horizontal axis (*yellow spots*), point of half-density defining each edge of the raphe (*green lines*), and tangent to the local nerve fiber bundle direction (*blue lines*). Each shape parameter was assessed in 2° increments of eccentricity, within a box 2° wide (*red*).

Temporal Raphe Assessment

OCT data was acquired with a Heidelberg SPECTRALIS with the Glaucoma Module (Heidelberg Engineering GmBH, Heidelberg, Germany). Following our previously published method,[13] the temporal raphe was assessed in the right eye from 2 partially overlapping, vertical, high density cube scans (11 μm separation, 10° width × 15° height). Fixation was guided by the internal spot within the device, and the acquisition region was finetuned relative to the spot by moving the position of the acquisition window in the Spectralis software (Heidelberg). Each high density scan required approximately 5 minutes acquisition time, dependent on fixation quality. En face intensity images were generated at the RNFL and montaged to cover an area from the fovea to at least 15° temporal.

The apparent axis of symmetry (midpoint) of the raphe was independently labeled by each of three experienced graders at 4 locations across the image. Exported intensity images at the level of the NFL were annotated in Adobe Photoshop CS2 (Adobe Systems, San Jose, CA, USA). Subjects were instructed to imagine the raphe as a straight line (example shown in magenta in Fig. 1B) and to label points that best represented the trajectory of this line. Labels were spaced evenly, subject to limitations arising from reflective artifacts at the RNFL. The

TABLE. Participant Details ($N = 78$)

Parameter	Mean ± SD	Range
Age (y)	25 ± 5	18 to 35
Sex (% female)	62%	–
Axial length (mm)	24.7 ± 1.5	21.3 to 28.8
Vitreous chamber depth (mm)	17.4 ± 1.5	14.5 to 21.4
Spherical equivalent (D)	−3.75 ± 2.75	−13.0 to 0.0
Fovea-disc angle (°)	−7.0 ± 3.8	−14.9 to 2.9
Fovea-raphe angle (°)	0.9 ± 3.4	−5.6 to 10.1
Disc-fovea-raphe angle (°)	172.0 ± 3.7	161.0 to 180.3

average angle formed between each label and the foveal center was calculated to estimate overall raphe orientation.

Anatomical angles are illustrated in Figure 1A and described previously.[13] The angle between fovea, disc, and horizontal axis was automatically determined by the Spectralis assessment of Bruch's membrane opening (BMO), with manual adjustment and confirmation by the operator. We term this the "fovea-disc" angle, with negative sign indicating a fovea inferior to the disc. The angle between the fovea, temporal raphe, and horizontal axis is the "fovea-raphe" angle, with positive sign indicating a raphe that slopes upward, away from the fovea. The angle between the three anatomical structures is the "disc-fovea-raphe" angle.

Raphe shape was characterized in greater depth as illustrated in Figure 1B (yellow, green, and blue markings). In 2° increments of eccentricity, within a box 2° in width (red), the graders each marked (1) the central axis of the raphe (yellow), (2) the point at which RNFL density appeared half-maximal (green), and (3) the tangent to the nerve fiber bundle trajectory (blue). If the relevant parameter could not be assessed, no label was made. Cronbach's alpha[27] showed strong agreement (0.92) between graders for labeling the raphe center, with moderate agreement for the raphe boundary (0.71) and nerve fiber bundle orientation (0.66). The grader's labels were averaged to reduce the influence of subjectivity.

To estimate statistical power for comparisons specifically between the emmetropic and high axial myopia sub-groups referred to above ($n = 12$ per group), we considered previously published figures for the standard deviation in raphe angle (3.2°)[14] and width of the raphe "gap" (0.37°).[11] These figures indicate that a difference in group means should be detectable (Type I error <0.05, Type II error <0.20) if on the order of 3.9° and 0.45°, respectively. These figures are within clinically significant margins: for the raphe angle, a rotation of 6.3° is sufficient to "flip" one of the (27.3) points of the SITA 24-2 test to the other side of the raphe; for the raphe gap, a difference of approx. 1.2° between normals and mild glaucoma has been reported,[11] based on a similar sample size.

RNFL Thickness Assessment

Peripapillary RNFL thickness and MRW were assessed using the Spectralis OCT Glaucoma Module (Heidelberg), which provides 360° assessment of nerve fiber thickness, respectively, surrounding the disc (we used the scan positioned 3.5 mm from the BMO center) or at the edge of the neuroretinal rim (shortest distance from local BMO to anterior extent of RNFL). The standard Spectralis analysis groups RNFL measurements according to the Garway-Heath sectors,[28] albeit rotated to account for each subject's individually measured fovea-disc axis. We grouped the superotemporal and superonasal sectors to create a superior sector, and the inferotemporal and inferonasal sectors to create an inferior sector, for direct comparison to the ISNT rule and related rules. The key structures and sectors are illustrated in Figure 1A.

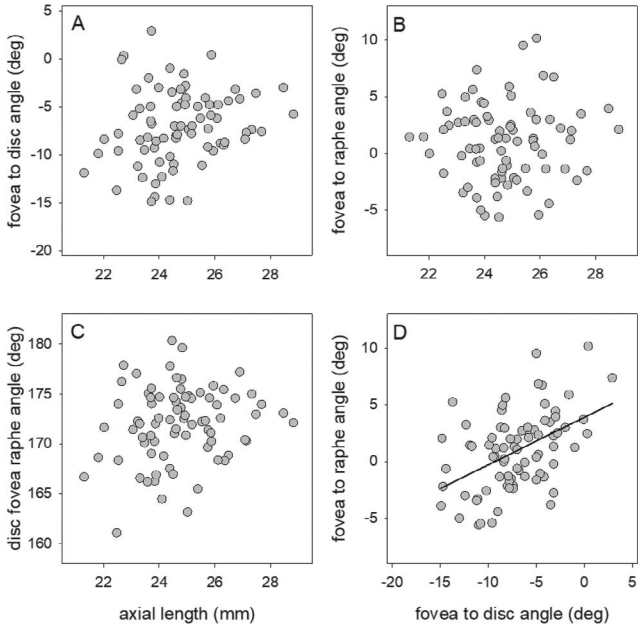

FIGURE 2. Relative orientation of the fovea, disc and temporal nerve fiber raphe as a function of axial length of the eye. (**A**) Angle formed between the fovea, disc and horizontal axis, abbreviated to "fovea-disc." (**B**) Angle formed between the fovea, raphe and horizontal image axis, abbreviated to "fovea-raphe" angle. (**C**) Angle formed between the disc, fovea, and temporal raphe, abbreviated to "disc-fovea-raphe." (**D**) Relationship between fovea-raphe and fovea-disc angles. Less superior insertion of the disc (positive fovea-disc angle) is partially compensated by a more superior orientation of the temporal raphe ($P < 0.0001$, $R^2 = 0.22$).

RESULTS

Relevant parameters for our participants are summarized in the Table, showing a wide range in degree of myopia and in relative orientations of the fovea, disc, and temporal raphe.

Figure 2 shows the influence of axial length on the fovea-disc angle (Fig. 2A), the fovea-raphe angle (Fig. 2B), and the disc-fovea-raphe angle (Fig. 2C). There was no significant Pearson correlation among any of the anatomical angles shown and the degree of myopia, whether measured by axial length ($P > 0.08$) or vitreous chamber depth ($P > 0.14$).

Figure 2D shows the relationship between the fovea-disc and fovea-raphe angles. As reported previously,[11,14] these parameters are moderately correlated ($P < 0.0001$, $R^2 = 0.22$) whereby a more inferior insertion of the disc is partially compensated by a more superior temporal raphe orientation.

Figure 3 plots various raphe shape parameters as a function of eccentricity for the 78 subjects. Figure 3A shows the location of the central axis of the raphe, expressed as a displacement from the horizontal axis passing through the fovea (i.e., the fovea is at 0°; superior displacements are positive). Axial length is coded, in ascending order, by both spot color (blue to red) and spot size (small to large). Raphe displacement was not significantly correlated with axial length at any eccentricity (8 independent Pearson correlations, $P > 0.11$). Considering only the emmetropic and high axial myopia groups, within the central 15° from fixation overall mean difference was <0.2°; within-eccentricity differences were no more than 0.3° between these groups and did not reach

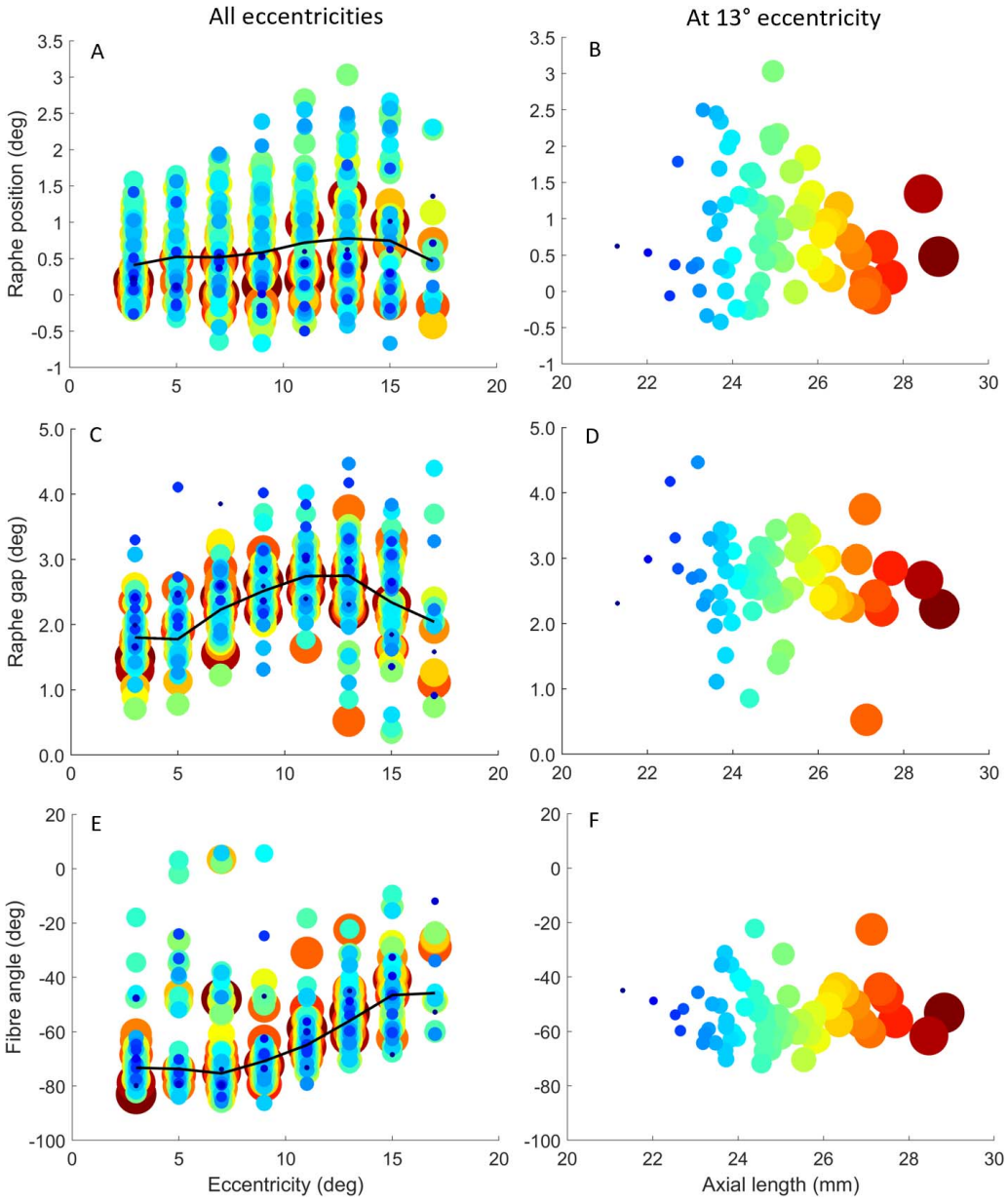

Figure 3. Geometry of the temporal nerve fiber raphe as a function of eccentricity, showing no significant association with axial length. Axial length is indicated by both the color and size of the filled circles, with longer eyes shown as redder and larger. (**A**) Displacement of the central point of the raphe from the horizontal axis passing through the fovea (i.e., fovea is at 0°; positive values indicate superior displacements). (**B**) As for A but considering only data at 13° eccentricity, now plotted as a function of axial length. (**C**) Apparent width of the raphe. (**D**) As for C but considering only data at 13° eccentricity, now plotted as a function of axial length. (**E**) Trajectory of fiber bundles. (**F**) As for E but considering only data at 13° eccentricity. Error bars show ± 1 SEM.

significance at the 95% level (Student's *t*-test with Bonferroni correction for the number of eccentricities considered). The most significant difference between these groups was apparent at 13° eccentricity, data for which is plotted in Figure 3B, confirming a lack of correlation.

Figure 3C shows raphe width at half visibility. Average width peaked at approximately 11°–13° from the fovea with a full-width at half maximum of 2.5°–3°, and decayed from there. Raphe width was significantly correlated with axial length only at 3° eccentricity ($P < 0.01$), however the correlation was weak ($R^2 = 0.10$) and was no longer significant ($P > 0.05$) after Bonferroni correction for the number of eccentricities considered. Considering only the emmetropic and high axial myopia groups, within the central 15° from fixation, overall mean difference was <0.4°; within-eccentricity differences were no more than 0.7° between these groups and did not reach significance at the 95% level (Student's *t*-test with Bonferroni correction for the number of eccentricities considered). The most significant difference between these groups was apparent at 13° eccentricity, data for which is plotted in Figure 3D, confirming a lack of correlation.

Figure 3E shows fiber bundle orientation relative to the vertical direction. As expected, fiber bundle orientation near the fovea was relatively close to vertical and transitioned toward being more horizontal, reaching an orientation of 45° at approximately 15°–17° eccentricity. Fiber orientation was not significantly correlated with axial length at any eccentricity (8 independent Pearson correlations, $P > 0.14$). Considering only

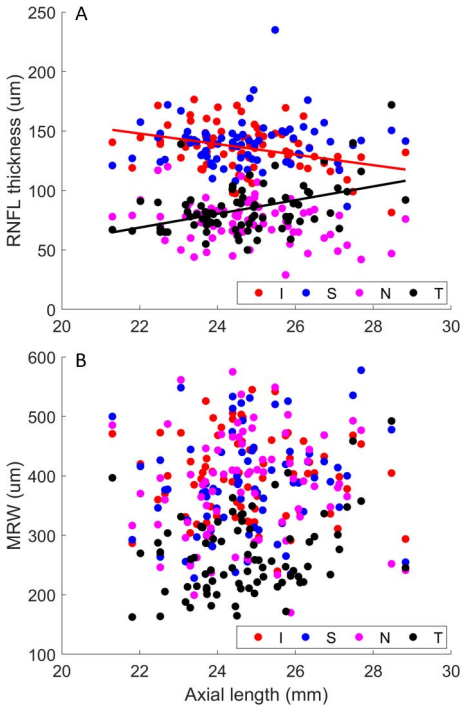

FIGURE 4. Papillary and peripapillary thickness of the retinal nerve fiber layer in 4 quadrants (inferior, superior, nasal, temporal) as a function of axial length. (**A**) RNFL thickness measured 3.5 mm from the disc. Inferior and temporal quadrant thicknesses were negatively ($P = 0.001$, $R^2 = 0.13$), and positively ($P = 0.0001$, $R^2 = 0.18$) associated with axial length, respectively. (**B**) Minimum rim width (MRW) measured at the disc. No significant correlation with axial length was evident.

the emmetropic and high axial myopia groups, within the central 15° from fixation, overall mean difference between groups was ~1°. Within-eccentricity differences were no more than ~10° and did not reach significance at the 95% level (Student's *t*-test with a Bonferroni correction for the number of eccentricities considered). The most significant difference between these groups was apparent at 13°, data for which is plotted in Figure 3F, confirming a lack of correlation.

Figure 4 shows the thickness of retinal nerve fiber layers at and near the disc as a function of axial length, for I, S, N, and T quadrants. Figure 4A shows RNFL thickness 3.5 mm from the disc, with a significant trend appearing only for inferior ($P = 0.001$) and temporal ($P = 0.0001$) quadrants after Bonferroni correction for multiple comparisons by a factor of 8 (S/N/I/T compared for both RNFL and MRW). Because these associations are in opposite directions, they may have ramifications for ISNT and related rules, as explored below. No other significant associations with axial length were noted (independent Pearson correlation for both metrics in 4 quadrants, Bonferroni corrected by a factor of 8 for the number of comparisons made).

Figure 5 shows the applicability of various rules of thumb for distribution of papillary and peripapillary nerve fibers as measured in our subjects. Probit regression was used to fit the underlying binary rule concordance. High concordance over the full range of axial lengths is evident for the T thinnest (MRW only) and IT rules (both MRW and RNFL). In general, there was a trend for reduced concordance with increasing axial length across the evaluated rules; due to the wide uncertainty of the curve fits, this relationship was only significant in our dataset for the T thinnest rule ($P < 0.005$ for RNFL and $P < 0.05$ for MRW).

Consideration of the binary rule concordance data for emmetropic and high axial myopia subgroups supports the probit analysis. The ISNT rule was followed a majority of the time in the emmetropes for both MRW (58%) and RNFL (67%), and a minority of the time in the highly myopic group (17% for MRW, 8% for RNFL). High concordance was obtained in the high myopia group with the T thinnest rule for MRW only (RNFL = 17%, MRW = 83%), and with the IT rule for both MRW and RNFL (MRW = 92%, RNFL = 75%).

Finally, no significant association was found between raphe orientation and the papillary/peripapillary nerve fiber measures ($P > 0.29$ for 16 individual regressions of fovea-raphe or fovea-disc-raphe against RNFL or MRW in each quadrant). This is unsurprising because such a link (1) was not evident previously for the non-myopic eye[14] and (2) would not be expected to develop in the present subject pool, given that raphe shape measures did not appear to be associated with axial length, as reported above.

DISCUSSION

This study evaluated nerve fiber geometry across a range of axial lengths, using custom high-density OCT scans across approximately 15°. Our study is the first to look systematically at the impact of myopia on nerve fiber bundle geometry at the temporal raphe. We found no significant relationship between the geometry of the temporal raphe and axial length of the eye. In regard to the nerve fiber layer thickness at and near the disc, consistent with previous work, we found that several rules of thumb (such as the ISNT rule) hold less frequently in more myopic eyes, with the exception of the IT rule for peripapillary RNFL and the IT and T thinnest rules for papillary NFL.

Trajectory of Temporal Retinal Nerve Fiber Bundles

Here, we present a more detailed framework for analysis of raphe orientation and shape than previously reported. Comparison between emmetropes and high axial myopes showed that axial elongation did not increase the apparent raphe gap; indeed, the trend was for a slightly narrower gap in high myopes. There was also minor superior displacement of the raphe in the parafoveal region (≤0.3° on average). These differences seem unlikely to be of practical significance. It should also be noted that angular units correspond to greater physical distance in a longer eye; for example, the angular extent of the raphe was narrowed ~20% in the high axial myopic group as compared to the emmetropic group; this equates to near-identical physical extent after adjusting for the 19% difference in axial length between the groups (27.2 mm vs. 22.9 mm). Therefore, our data are consistent with negligible physical remodeling of the raphe as a result of increases in axial length due to myopia.

This study confirmed our previous observation of significant correlation between the orientation of the raphe and disc relative to the fovea.[14] Specifically, when the disc is inserted less superiorly, the raphe tends to be tilted more superiorly, partially conserving the anatomical angle between the disc, fovea, and temporal raphe. There was, in turn, a mild correlation between axial length and the fovea-disc angle; however, this did not manifest in any direct correlation between axial length and raphe orientation. A potential caveat to the observed correlation between the above anatomical angles is any rotational error in positioning the subject's head for imaging; rotation of the head would cause all angles to rotate together, thereby artificially increasing the correlation coefficient between them. However, test-retest errors for

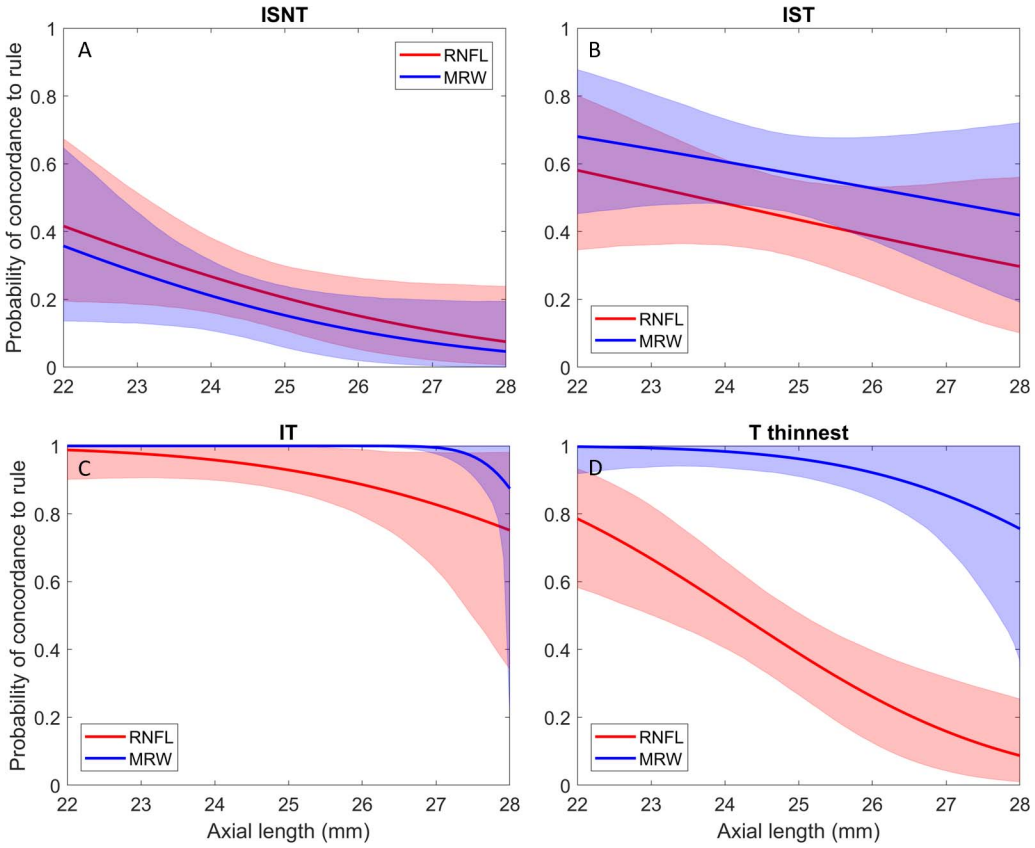

Figure 5. Probit regression of concordance data for ISNT and related rules as a function of axial length. Solid lines show best fit for the RNFL (*red*) and MRW (*blue*) measures. Shaded regions indicate 95%CI on fitted curves following bootstrap by subject 10 000 times with replacement; *magenta-shaded* regions indicate overlap between the RNFL and MRW confidence intervals. (**A**) Fit for the I > S > N > T rule. (**B**) Fit for the I > S > T rule. The I > S rule is not depicted here, but results looked almost identical to the I > S > T rule. (**C**) Fit for the I > T rule. (**D**) Fit for the T thinnest rule.

angular measures of the kind considered here are approximately ±1°,[19] which is far less than the variance observed in our data (see Fig. 2D).

We also confirm our previous observation that in a minority of eyes, the temporal raphe deviates sufficiently from horizontal to result in flipping the mapping between visual field location and expected superior/inferior ONH hemifield.[18] In the present dataset, 5 participants had sufficiently non-horizontal raphe angles to result in aberrant structure-function mapping for the most nasal points of the 24-2 and 10-2 visual field maps (Humphrey Field Analyzer, Carl Zeiss, Dublin, CA, USA). The refractive error of these individuals ranged from −1.25 to −8.5D. In these individuals, conventional mapping of structure function is likely to prove problematic (it should be noted that our measurements of raphe geometry did not extend beyond 15°; the above interpretation requires extrapolation of the raphe trajectory to 27° eccentricity).

Recent work tracing RNFL bundles across the posterior pole from conventional fundus photographs indicates that race of the participant may be an important contributor to variability between highly myopic individuals.[29] Our study was not designed nor powered to consider the contribution of race. Given the difficulty in tracing RNFL trajectory remotely from the disc with fundus photography,[30] the shape characterization approach presented here may prove useful in further exploring the contribution of racial differences in explaining variability encountered in high myopia.

Adaptive optics retinal imaging studies have shown that, in and around the fovea, axial elongation of the eye in myopia is generally such that the angular spacing between adjacent cone photoreceptors remains constant (i.e., physical density is reduced, consistent with a geometric "stretch" of the globe).[31–33] Psychophysical measurements of resolution acuity and spatial summation in myopic eyes are consistent with a reduction in retinal ganglion cell density, over and above that implied from such a "simple" physical stretch.[34,35] The results of the present study indicate that, in angular units, the geometry of retinal nerve fiber bundles was not differentiable between highly myopic and nonmyopic eyes. This indicates that any purported reduction in the density of ganglion cells was not accompanied by a reduction in the density of nerve fiber bundles (or alternately, that the angular density of retinal ganglion cells does not, in fact, decrease with axial length). Caution should be exercised when interpreting this result, since it could also be explained by a concomitant change in packing density of fibers within a bundle, an increase in bundle visibility compared with the emmetropic eye, or that ganglion cell density does decrease but not at the temporal raphe.

Thickness of Papillary and Peripapillary Nerve Fibers

There is relatively little difference in thickness between ONH quadrants that are compared by ISNT and related rules (for example, see Fig. 4). For this reason, such rules may be very sensitive to slight losses in disease; equally, they may show a high false positive rate due to natural variability between individuals, measurement error, or small nonpathological loss. This makes it important to establish how robustly the ISNT rule is obeyed in the healthy, nonglaucomatous eye. Recent studies

have attempted to answer this question and observed that, contrary to clinical wisdom, the rule is more often than not disobeyed even in healthy eyes.[5] Our results echo this sentiment in eyes with emmetropia or low myopia, showing that the problem may be compounded in eyes suffering from higher myopia. This finding supports another recent study published on a large myopic cohort.[6]

For the RNFL, lower concordance in myopia may be explained by a tendency for temporal RNFL to become thicker with higher axial length, while inferior RNFL became thinner (Fig. 4). Although the observed correlation does not account for a large proportion of the variance, the similar baseline thickness of superior/inferior and nasal/temporal RNFL, noted above, means that small changes can cause failure of simple rules of the type considered here. For MRW, no significant associations were found with axial length, which may explain the generally higher rates of concordance observed for rules based on MRW. Rather than quadrant thickness, other studies have examined the location of peak thickness in the peripapillary RNFL[7,8]; a broad pattern of results is the temporal movement of superior and inferior peaks in RNFL density. In accord with the findings of the present study, this would tend to reduce thickness of vertical quadrants and increase thickness for the temporal quadrant.

A higher rate of ISNT rule concordance, and corresponding specificity for diagnosis of glaucoma, has been recently demonstrated for MRW when compared with traditional evaluation of the neuroretinal rim in color fundus photography.[36] Our results showed a trend of higher concordance for rules based on MRW as compared to those based on RNFL thickness; this difference became significant for the T thinnest rule (Fig. 5). For the IT rule in the high axial myopes, reasonable concordance was apparent for both measures of MRW (>92%) and RNFL (>75%). Of course, the improved specificity for these metrics is only relevant to the management of glaucoma if sensitivity is high, which awaits further study. Regardless, the present study shows that use of the ISNT rule for the peripapillary RNFL should not be applied to highly myopic eyes.

Overall Implications

Overall, this study observed little influence of axial length on the course of nerve fibers in the temporal raphe region but did show some differential effects on the thickness of papillary and peripapillary nerve fibers. Previous studies have observed a shift in the peak of the peripapillary thickness profile with axial length[7,8]; this may produce some expectation that the trajectory of nerve fibers across the papillomacular area must be altered in order to produce the observed finding. Our results are not inconsistent with this since we only analyzed the shape of the raphe and not the full arc of fibers traversing the retina; however, the results do demonstrate that any readjustment of fiber trajectories would not seem to include the temporal raphe (to within the power of our study). Indeed, we did not find any association between the thickness of papillary and peripapillary nerve fibers and the geometry of the raphe. Our study also did not consider the influence of race in the highly myopic eye, which may alter the trajectory of retinal nerve fibers, as mentioned above.[29]

The geometry of the temporal raphe has been argued to be relevant for accurate assessment of visual field loss in glaucoma and marriage of perimetric and structural data from OCT. The present study, while confirming previous reports of high interindividual variability in raphe geometry, demonstrates that systematic adjustment for the degree of myopia is not required for this endeavor.

However, consistent with other studies, high myopia does alter the expected pattern of nerve fiber layer thickness at and near the disc; these changes occur in such a way that commonly employed rules of thumb (such as the ISNT rule) become less likely to hold true. The present study suggests alternate strategies with improved specificity in healthy eyes; however, further study would be needed to gauge their sensitivity to glaucoma. In the meantime, use of the ISNT rule applied to the peripapillary RNFL should be avoided in the assessment of glaucoma in high myopia.

Acknowledgments

Supported by Australian Research Council (ARC) Linkage Project LP13100055 funding and research support from Heidelberg Engineering GmbH, Heidelberg, Germany. The sponsor and funding organization had no role in the design or conduct of this research.

Disclosure: **P. Bedggood**, None; **S. Mukherjee**, None; **B.N. Nguyen**, None; **A. Turpin**, Heidelberg Engineering GmbH (F), Haag-Streit AG (F), CenterVue SpA (C); **A.M. McKendrick**, Heidelberg Engineering GmbH (F); Haag-Streit AG (F), CenterVue SpA (C)

References

1. Mitchell P, Hourihan F, Sandbach J, Wang JJ. The relationship between glaucoma and myopia: the Blue Mountains Eye Study. *Ophthalmology*. 1999;106:2010–2015.
2. Quigley HA, Addicks EM, Green WR. Optic nerve damage in human glaucoma: III. Quantitative correlation of nerve fiber loss and visual field defect in glaucoma, ischemic neuropathy, papilledema, and toxic neuropathy. *Arch Ophtalmol*. 1982; 100:135–146.
3. Jonas JB, Budde WM. Diagnosis and pathogenesis of glaucomatous optic neuropathy: morphological aspects. *Prog Retin Eye Res*. 2000;19:1–40.
4. Medeiros FA, Zangwill LM, Bowd C, Vessani RM, Susanna R Jr, Weinreb RN. Evaluation of retinal nerve fiber layer, optic nerve head, and macular thickness measurements for glaucoma detection using optical coherence tomography. *Am J Ophthalmol*. 2005;139:44–55.
5. Poon LY-C, Solá-Del Valle D, Turalba AV, et al. The ISNT rule: how often does it apply to disc photographs and retinal nerve fiber layer measurements in the normal population? *Am J Ophthalmol*. 2017;184:19–27.
6. Qiu K, Wang G, Lu X, Zhang R, Sun L, Zhang M. Application of the ISNT rules on retinal nerve fiber layer thickness and neuroretinal rim area in healthy myopic eyes. *Acta Ophthalmol*. 2018;96:161–167.
7. Leung CK-S, Yu M, Weinreb RN, et al. Retinal nerve fiber layer imaging with spectral-domain optical coherence tomography: interpreting the RNFL maps in healthy myopic eyes. *Invest Ophthalmol Vis Sci*. 2012;53:7194–7200.
8. Yamashita T, Asaoka R, Kii Y, Terasaki H, Murata H, Sakamoto T. Structural parameters associated with location of peaks of peripapillary retinal nerve fiber layer thickness in young healthy eyes. *PLoS One*. 2017;12:e0177247.
9. Vrabec F. The temporal raphe of the human retina. *Am J Ophthalmol*. 1966;62:926–938.
10. Huang G, Gast TJ, Burns SA. In vivo adaptive optics imaging of the temporal raphe and its relationship to the optic disc and fovea in the human retina. *Invest Ophthalmol Vis Sci*. 2014; 55:5952–5961.
11. Huang G, Luo T, Gast TJ, Burns SA, Malinovsky VE, Swanson WH. Imaging glaucomatous damage across the temporal raphe. *Invest Ophthalmol Vis Sci*. 2015;56:3496–3504.

12. Chauhan BC, Sharpe GP, Hutchison DM. Imaging of the temporal raphe with optical coherence tomography. *Ophthalmology* 2014;121:2287–2288.
13. Bedggood P, Tanabe F, McKendrick AM, Turpin A. Automatic identification of the temporal retinal nerve fiber raphe from macular cube data. *Biomed Opt Express*. 2016;7:4043–4053.
14. Bedggood P, Nguyen B, Lakkis G, Turpin A, McKendrick AM. Orientation of the temporal nerve fiber raphe in healthy and in glaucomatous eyes. *Invest Ophthalmol Vis Sci*. 2017;58:4211–4217.
15. Åsman P, Heijl A. Glaucoma hemifield test: automated visual field evaluation. *Arch Ophtalmol*. 1992;110:812–819.
16. Naghizadeh F, Holló G. Detection of early glaucomatous progression with octopus cluster trend analysis. *J Glaucoma*. 2014;23:269–275.
17. Yamashita T, Sakamoto T, Kakiuchi N, Tanaka M, Kii Y, Nakao K. Posterior pole asymmetry analyses of retinal thickness of upper and lower sectors and their association with peak retinal nerve fiber layer thickness in healthy young eyes. *Invest Ophthalmol Vis Sci*. 2014;55:5673–5678.
18. McKendrick AM, Denniss J, Wang YX, Jonas JB, Turpin A. The proportion of individuals likely to benefit from customized optic nerve head structure-function mapping. *Ophthalmology*. 2017;124:554–561.
19. Denniss J, Turpin A, McKendrick AM. Individualized structure–function mapping for glaucoma: practical constraints on map resolution for clinical and research applications. *Invest Ophthalmol Vis Sci*. 2014;55:1985–1993.
20. Hood DC, Raza AS, de Moraes CGV, Liebmann JM, Ritch R. Glaucomatous damage of the macula. *Prog Retin Eye Res*. 2013;32:1–21.
21. Ashimatey BS, King BJ, Malinovsky VE, Swanson WH. Novel technique for quantifying retinal nerve fiber bundle abnormality in the temporal raphe. *Optom Vis Sci*. 2018;95:309.
22. Mori S, Kurimoto T, Kanamori A, et al. Discordance of disc-fovea raphe angles determined by optical coherence tomography and MP-3 microperimetry in eyes with a glaucomatous hemifield defect. *Invest Ophthalmol Vis Sci*. 2019;60:1403–1411.
23. Hart WM, Becker B. The onset and evolution of glaucomatous visual field defects. *Ophthalmology*. 1982;89:268–279.
24. Tanabe F, Matsumoto C, McKendrick AM, Okuyama S, Hashimoto S, Shimomura Y. The interpretation of results of 10-2 visual fields should consider individual variability in the position of the optic disc and temporal raphe. *Br J Physiol Opt*. 2018;102:323–328.
25. Kleinstein RN, Jones LA, Hullett S, et al. Refractive error and ethnicity in children. *Arch Ophthalmol*. 2003;121:1141–1147.
26. Friedman NJ, Kaiser PK. *Essentials of Ophthalmology*. Philadelphia, PA: Elsevier Health Sciences; 2007.
27. McGraw KO, Wong SP. Forming inferences about some intraclass correlation coefficients. *Psychol Methods*. 1996;1:30.
28. Garway-Heath DF, Poinoosawmy D, Fitzke FW, Hitchings RA. Mapping the visual field to the optic disc in normal tension glaucoma eyes. *Ophthalmology*. 2000;107:1809–1815.
29. Qiu K, Zhang M, Wu Z, et al. Retinal nerve fiber bundle trajectories in Chinese myopic eyes: comparison with a Caucasian based mathematical model. *Exp Eye Res*. 2018;176:103–109.
30. Denniss J, Turpin A, Tanabe F, Matsumoto C, McKendrick AM. Structure–function mapping: variability and conviction in tracing retinal nerve fiber bundles and comparison to a computational model. *Invest Ophthalmol Vis Sci*. 2014;55:728–736.
31. Chui TYP, Song H, Burns SA. Individual variations in human cone photoreceptor packing density: variations with refractive error. *Invest Ophthalmol Vis Sci*. 2008;49:4679–4687.
32. Legras R, Gaudric A, Woog K. Distribution of cone density, spacing and arrangement in adult healthy retinas with adaptive optics flood illumination. *PLoS One*. 2018;13:e0191141.
33. Li KY, Tiruveedhula P, Roorda A. Intersubject variability of foveal cone photoreceptor density in relation to eye length. *Invest Ophthalmol Vis Sci*. 2010;51:6858–6867.
34. Atchison DA, Schmid KL, Pritchard N. Neural and optical limits to visual performance in myopia. *Vision Res*. 2006;46:3707–3722.
35. Chui TY, Yap MK, Chan HH, Thibos LN. Retinal stretching limits peripheral visual acuity in myopia. *Vision Res*. 2005;45:593–605.
36. Park DY, Lee EJ, Han JC, Kee C. Applicability of ISNT rule using BMO-MRW to differentiate between healthy and glaucomatous eyes. *J Glaucoma*. 2018;27:610–616.

Investigative Ophthalmology & Visual Science